Proceedings of the West Virginia Academy of Science

Original Research Paper

Experimental and Computational Analysis of a Shell-and-Tube Heat Exchanger for Performance Optimization

Maya Panta[1], V'yacheslav (Slava) Akkerman[2], Yogendra Panta[3*]

[1] *Woodrow Wilson High School, Beckley, WV, USA, graduated Spring 2026. Future affiliation: Department of Mechanical and Aerospace Engineering, School of Engineering and Applied Science, Princeton University, Princeton, NJ, USA, beginning Fall 2026.*

[2] *Department of Mechanical, Materials and Aerospace Engineering, West Virginia University (WVU), Morgantown, WV, USA.*

[3] *Leonard C. Nelson School of Engineering, WVU Institute of Technology, Beckley, WV, USA.*

Article history
Received: 28 October 2025
Revised: 11 July 2026
Accepted: 13 July 2026

**Corresponding Author*:
Yogendra Panta, WVU Institute of Technology, Beckley, USA;
Email: ympanta@mail.wvu.edu

Abstract: Heat exchangers are devices designed to transfer heat energy between fluids through conduction and convection. Among various configurations, the shell-and-tube design is one of the most common. It consists of a shell containing a bundle of parallel tubes, where two fluids at different temperatures flow: one through the tubes and the other around them, exchanging heat energy in the process. This configuration is widely used in petrochemical processing, oil rigs, and other high-pressure industrial environments. In this study, an Armfield HT33X shell-and-tube heat exchanger was experimentally tested in a countercurrent configuration, with hot water flowing through the tubes and cold water flowing through the shell. The hot-water flow rate was varied to evaluate its effect on outlet temperatures, thermal efficiency, and effectiveness. A simplified ANSYS Fluent finite-volume model was then used to compare the experimental trend and identify flow and thermal-field features that may limit performance. The experimental results showed that increasing the hot-water flow rate generally increased thermal effectiveness, with a peak experimental value of approximately 0.22. The computer simulation model predicted the same general trend but a higher peak value of approximately 0.28; therefore, the simulation is interpreted as a qualitative diagnostic and trend-comparison tool rather than exact validation. Preliminary MATLAB effectiveness-NTU screening suggests that surface-area enhancement and improved shell-side flow guidance could increase theoretical effectiveness, but the proposed redesign requires future seven-tube conjugate heat-transfer CFD and experimental validation before quantitative performance claims can be made.

Keywords: Shell-and-Tube Heat Exchanger; Heat Exchanger Effectiveness; ANSYS Fluent; MATLAB; Experimental Testing; Surface-Area Enhancement; Flow Distribution

Introduction

Heat exchangers are essential devices that transfer heat energy from one fluid to another without mixing them directly. This is achieved via the heat transfer modes of (i) *conduction*, with heat flowing through a solid material, and (ii) *convection*, with heat transferred via circulating currents (convection currents) within fluids, respectively.

Heat can be transferred by such flow mechanisms as (i) counter flow, (ii) cross flow, and (iii) parallel flow, each of which plays a critical role in determining the thermal effectiveness of heat transfer. Specifically, (i) counter flow involves fluids flowing in opposite directions, maximizing heat transfer effectiveness; (ii) parallel flow occurs when both fluids move in the same direction; and (iii) cross flow involves fluids flowing perpendicular to each other. The choice of flow arrangement depends on the intended application for the desired effectiveness of the heat exchanger.

One frequently used type of heat exchanger is the shell-and-tube heat exchanger (STHE). It consists of a cylindrical shell that encloses a bundle of tubes, allowing one fluid to flow through the tubes and the other fluid to flow across the tube bundle. Because of its mechanical robustness and flexibility in pressure and temperature applications, the STHE remains common in process, power, and thermal-fluid systems (Kern, 1950; Kakaç and Liu, 2012; Bell, 2005).

Heat exchange is facilitated between fluid flowing through the shell and fluid flowing through the tubes. The design often incorporates baffles, strategically placed within the shell to manipulate the fluid flow, induce turbulence, and enhance thermal effectiveness of heat transfer. Within the STHE, radial conduction and convection in both fluids will assist heat transfer.

The STHEs are often used in industry to capture waste heat from industrial processes, thus improving energy efficiency and cost effectiveness. The most common applications include HVAC systems, nuclear power plants, turbine engines, and car radiators.

However, there are some disadvantages of STHE as compared to other types of heat exchangers such as vibrations, dead zones, high pressure drop, and larger size requirements.

Designing or modifying an STHE is complicated because heat-transfer area, baffle arrangement, pressure drop, material properties, fouling, and shell-side flow distribution interact with one another. Classical heat-exchanger design methods and recent Computational Fluid Dynamics (CFD) studies show that baffle layout and surface-area enhancement can strongly influence thermal performance (Incropera and DeWitt, 2006; Prithiviraj and Andrews, 1998; Tayyab et al., 2024; Mohammadzadeh et al., 2025).

In this study, CFD was used after experimental testing to visualize flow and temperature fields and to guide future design decisions. The CFD model is useful for diagnosing possible limitations, but it is not treated as a substitute for a geometrically matched, fully validated experiment.

Recent CFD tools allow complex heat-exchanger geometries to be discretized into computational cells so that governing conservation equations can be solved numerically. This capability supports detailed visualization of velocity, pressure, and temperature fields; however, CFD accuracy depends on appropriate geometry, boundary conditions, material properties, mesh quality, convergence behavior, and turbulence-model selection.

In this work, ANSYS Fluent's finite volume method (FVM) was used because it is a standard CFD approach for solving the conservation equations for fluid flow and heat transfer in discretized control volumes (ANSYS FLUENT Theory Guide, n.d.; Rodrigues and Srivastava, 2024).

The initial CFD model used the standard k-epsilon turbulence model available in ANSYS Fluent. Because shell-side flow in this small apparatus may be laminar or transitional, those CFD results are interpreted qualitatively; future high-fidelity simulations should use Reynolds-number-based model selection, including a laminar shell-side model and SST k-omega treatment for near-wall and transition effects where appropriate (Menter, 1994).

The objective of this study is to explore how an existing STHE can be redesigned to create a novel and more thermally effective solution, while maintaining its structural integrity.

To fulfill this objective, the study combined laboratory testing, a simplified CFD comparison, and preliminary MATLAB effectiveness-NTU screening. The experimental testing was used to observe how hot water flow-rate variation affected thermal performance. It was hypothesized that increasing the hot-water flow rate would increase the measured effectiveness. ANSYS Fluent was then used to compare experimental trends and visualize likely flow and thermal limitations. MATLAB calculations were used only as preliminary screening for possible surface-area and flow-guidance improvements, not as final validation of a redesigned exchanger.

Materials and Methods

Lab Experimentation

An Armfield Inc. HT33X shell-and-tube heat exchanger with a nominal heat-transfer area of 20,000 mm², a 44.45 mm shell diameter, seven tubes with 6.35 mm outside diameter, and six semicircular baffles was configured for countercurrent operation and connected to an HT30X Heat Exchanger Service Unit and Graphic User Interface (GUI) computer. The apparatus was operated according to the counterflow Exercise A procedure in the equipment manual.

Before turning on the apparatus, the pressure regulator was adjusted, and the GUI was connected via cord to the HT30X unit. Additionally, the fluid circuits were snugly connected into inlet ports, outlets, and the tap where water is sourced, ensuring hot water flows through the tubes and cold water flows through the shell. After plugging in the apparatus, it was switched on and configured to Countercurrent Operation and Exercise A.

Hot water set to a control temperature of ~ 50 °C ran through the tubes of the unit, whereas cold water set to a control temperature of ~ 15.7 °C ran through the shell of the unit, passing over the hot tubes several times to facilitate heat transfer.

The cold-water valve setting was kept constant throughout the experiment, with a flow rate of approximately 1.35 L/min. The hot-water flow rate was varied from 0.5 to 5.0 L/min in 0.5 L/min increments to identify its effect on outlet temperatures and calculated performance. After each flow-rate adjustment, pressure and temperature readings were monitored until they stabilized before data collection. Three trials were recorded at each hot-water flow rate.

The data were collected at four temperature points: T_1 (hot water inlet port), T_2 (hot water outlet port), T_3 (cold water inlet port), and T_4 (cold water outlet port), and two flow rate points: q_h (hot water inlet flow rate) and q_c (cold water inlet flow rate).

Calculations

Following data collection, the quantities used to evaluate heat-exchanger performance were calculated using the equations below. The associated experimental parameters are summarized in **Table 1**.

1. Mass flow rate:

$$\dot{m} = q.\rho \tag{1}$$

where q is volumetric flow rate and ρ is fluid density.

2. Ambient heat gain through the acrylic shell:

$$Q_a = \frac{2\pi k_s L(T_a - T_3)}{ln(D_o/D_i)} \tag{2}$$

where k_s is the acrylic-shell thermal conductivity, T_a is the room-air temperature, T_3 is the cold-water inlet temperature, L is the shell length; D_o and D_i are the outside and inside shell diameters, respectively. Tube diameters are denoted separately as d_o and d_i.

3. Total heat gained by the cold-water stream:

$$Q_c = \dot{m}_c C_{p,c}(T_4 - T_3) \tag{3}$$

4. Estimated heat gained by the cold water

from the hot-water stream:

$$Q_r = Q_c - Q_a \tag{4}$$

5. Heat-capacity rate:

$$C = \dot{m}C_p \tag{5}$$

where C_{min} is the smaller of the hot- and cold-side heat-capacity rates:

$$C_{min} = min(C_h, C_c) \tag{6}$$

$$C_h = \dot{m}_h C_{p,h}, C_c = \dot{m}_c C_{p,c} \tag{7}$$

6. Heat emitted by the hot water:

$$Q_e = \dot{m}_h C_{p,h}(T_1 - T_2) \tag{8}$$

7. Overall thermal effectiveness:

$$\varepsilon = \frac{Q_r}{C_{min}(T_1 - T_3)} \tag{9}$$

8. Overall thermal efficiency:

$$\eta = \frac{Q_r}{Q_e} \times 100\% \tag{10}$$

Statistical Methods

Data are presented as means ± SD from three trials at each flow rate. Trend lines and goodness-of-fit values were used to compare experimental and simulation trends, and values differing by more than ±5% from the local trend were treated cautiously as potential outliers. Because full calibrated instrument uncertainties were not available for all measured quantities, formal Kline-McClintock uncertainty propagation was not claimed; the reported results are therefore interpreted as trend-level findings rather than high-precision measurements.

ANSYS Fluent Simulation

Using the experimental boundary conditions, an ANSYS Fluent (2024 R2) model was configured to approximate the laboratory heat exchanger. The simulation was run for 5,000 solver iterations at each tested flow rate to compare the overall trend and examine temperature, velocity, and pressure fields. The model was not treated as a one-to-one validation model because the computational geometry did not exactly match the seven-tube experimental apparatus.

Table 1. Relevant Experimental Information

Water Properties
Density
Hot water flowing @ 50°C in each tube, ρ_h = 988 kg/m³ Cold water flowing at approximately 16 °C in the shell surrounding the outside of the tubes, ρ_c = 998.9 kg/m³
Specific Heat Capacity
Hot water flowing at approximately 50 °C in each tube, $C_{p,h}$ = 4178 J/(kg·K) Cold water flowing at approximately 16 °C in the shell surrounding the outside of the tubes, $C_{p,c}$ = 4185 J/(kg·K)
Surrounding Air Properties
Air temperature, T_a = 21.11 °C Density of room air, ρ_a = 1.2 kg/m³
Shell and Tube Geometries
Tube Geometry
Number of tubes, n = 7 Length of Tubes, L = 144 mm Outside diameter of each tube, d_o = 6.35 mm Inside diameter of each tube, d_i = 5.15 mm No. of Semi-circular Baffles = 6
Shell Geometry
Number of shells, n = 1 housing all seven tubes Length of the Shell, L = 144 mm Outside diameter of shell, D_o = 44.45 mm Inside diameter of shell, D_i = 43.95 mm Thermal conductivity of acrylic shell, k_s = 0.19 W/(m·K) Combined nominal heat-transfer area, A = 20,000 mm²

Simulation Setup

The computational geometry consisted of six horizontal steel tubes, an acrylic-plastic shell, and two separate fluid domains for the hot- and cold-water streams (**Figure 1**). The laboratory HT33X unit contains seven horizontal steel tubes; therefore, the computational model is a simplified representation of the experimental apparatus rather than a one-to-one geometric replica. Although the model was constructed to preserve an effective heat-transfer area close to the nominal value of 20,000 mm², this geometric simplification may influence local shell-side flow distribution, temperature contours, and quantitative comparison with experiment. Accordingly, this study interprets the CFD results primarily as qualitative flow and thermal-field diagnostics rather than exact validation of the laboratory unit. The properties of the fluids and materials are listed in **Table 2**.

The geometrical model was discretized using a hex-dominant mesh, with a maximum aspect ratio of 21.53 and a minimum orthogonal quality of 0.2 (**Figure 2**). Hot water was modeled in the tube-side fluid domain and cold water in the shell-side domain, consistent with the experimental flow arrangement. The mesh was refined near the inlet/outlet ports and wall boundaries to improve the qualitative resolution of flow and thermal-field patterns.

Several inlet and outlet boundary conditions were set as summarized in **Table 3**. The baffles, tubes, and partition walls were treated as no-slip walls with coupled thermal boundary conditions, while the tank, inlet, and outlet walls were modeled as no-slip adiabatic walls. Because the initial model used wall functions with a standard k-epsilon approach, the resulting near-wall and shell-side predictions are treated as preliminary and qualitative rather than definitive heat-transfer coefficients.

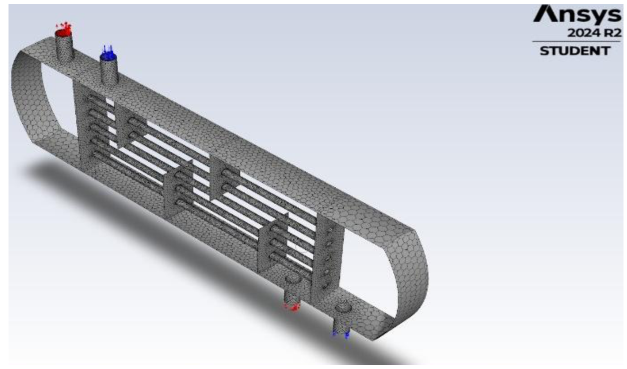

Figure 1. ANSYS Geometry of the STHE.

Figure 2. ANSYS Meshing of the STHE.

Table 2. Properties for Fluids and Materials Used in ANSYS Fluent Simulation.

	Hot Water in Tubes	Cold Water in the Shell	Steel Tubes	Acrylic-plastic Shell
ρ ($\frac{kg}{m^3}$)	988	998.2	8030	1180
C_p (J/(kg. K)	ǀ78	4185	502.5	1464
k (W/(m. K)	0.55	0.5	16.27	0.19
μ (N s/m²)	0.0005465	0.001108	N/A	N/A
MW (kg/kmol)	28.97	28.97	N/A	N/A

Where, ρ represents density, C_p represents specific heat capacity, k represents thermal conductivity, μ represents viscosity, and MW represents molecular weight.

Table 3. Inlet/Outlet Conditions Used in the Initial Simplified CFD Model.

	Shell Inlet	Tube Inlet	Both Outlets
Mass Flow Rate ($\frac{kg}{s}$)	0.0226	0.0494	N/A
Temperature (K)	289	323	N/A
Turbulent intensity (%)	5	5	N/A
Hydraulic Diameter (m)	0.03	0.03	N/A
Pressure Outlet (Pa)	N/A	N/A	0
Backflow Temperature (K)	N/A	N/A	284

The core conservation equations and heat-transfer relations used to interpret the simulation are summarized below. These equations are presented as editable Word equations. The CFD results remain qualitative because the geometry and turbulence-model assumptions were simplified relative to the physical seven-tube apparatus.

Continuity equation:

$$\frac{\partial \rho}{\partial t} + \nabla \cdot (\rho v) = 0 \quad (11)$$

Momentum equation:

$$\frac{\partial (\rho v)}{\partial t} + \nabla \cdot (\rho v v) = -\nabla p + \nabla \cdot \tau + \rho g \quad (12)$$

Energy equation:

$$\frac{\partial (\rho E)}{\partial t} + \nabla \cdot \left[v(\rho E + p)\right) = \nabla \cdot \left(k_{eff} \nabla T\right) + S_h \quad (13)$$

Heat-transfer relation:

$$Q = UA\Delta T_{lm} \quad (14)$$

Log-mean temperature difference:

$$\Delta T_{lm} = \frac{\Delta T_1 - \Delta T_2}{ln(\Delta T_1/\Delta T_2)} \quad (15)$$

Shaft work for the present analysis:

$$W = 0 \quad (16)$$

In these relations, ρ is density, v is velocity, p is pressure, τ is the stress tensor, E is total energy, k_{eff} is effective thermal conductivity, T is temperature, S_h is an energy-source term, U is the overall heat-transfer coefficient, A is heat-transfer area, and ΔT_{lm} is the log-mean temperature difference. Additional details on the finite-volume formulation, wall functions, and turbulence closure are available in the heat and fluid flow theory (*ANSYS FLUENT 12.0 Theory Guide,* n.d.).

The FVM simulation was run for 5,000 solver iterations at each experimental flow rate, with residual settings used to monitor numerical convergence. A relaxation factor of 0.25 was applied to higher-order terms to stabilize the solution process. Because the standard k-epsilon model can overpredict mixing in laminar or transitional regions, the CFD results are used in this paper as trend comparison and flow visualization, not as a final validated CFD model.

Post-Simulation

Following the simulations, residuals, heat fluxes, and mass-flow balances were reviewed to check numerical stability. Velocity, pressure, and temperature contours were then used to identify likely regions of stagnation, pressure loss, and uneven thermal distribution that could guide future optimization.

MATLAB Calculations

Following evaluation of the heat exchanger's performance, possible optimization areas were identified and conceptual design changes were screened. A published MATLAB effectiveness-NTU code (Kokate, 2020) was used to estimate how changes in effective heat-transfer area could influence effectiveness. These MATLAB results are preliminary design estimates and were not treated as CFD or experimental validation of the proposed new design.

Results

Experimental Results

Three trials were averaged for each tested hot-water flow rate, yielding one average value for each temperature point (T_1, T_2, T_3, and T_4) at each flow condition (**Table 4**). The cold-water flow rate, q_c, ranged from 1.33 to 1.38 L/min, the hot-water inlet temperature, T_1, ranged from 49.6 to 51.3 °C, and the cold-water inlet temperature, T_3, ranged from 15.7 to 15.8 °C.

Using the average experimental data in Table 4, effectiveness (ε), efficiency (η), and various other metrics were calculated.

During experimentation (**Figures 3 to 6**), air pockets/bubbles were observed in the shell side of the heat exchanger. These air pockets are treated as an experimental limitation because they can reduce effective liquid contact area, alter local heat transfer, and contribute to scatter in the measured temperatures. The ambient heat-gain term, Q_a, was therefore defined as heat transfer through the acrylic shell from the surrounding air, not as a correction for beneficial bubble-induced heat transfer. Future experiments should include more thorough purging/priming before data collection.

Thermal efficiency remained above 75% for all trials and generally increased with effectiveness. The highest calculated efficiency was 99%, the lowest value was 77%, and the average efficiency was approximately 90% (**Table 5**). These values indicate that the unit transferred a substantial fraction of the heat released by the hot stream under the tested conditions, even though the overall effectiveness remained low.

Thermal effectiveness increased as the hot-water flow rate increased, peaking at approximately 0.22 at hot-water flow rates of 4.5 L/min and 5.0 L/min. From 0.5 to 5.0 L/min, effectiveness increased by approximately 47%, supporting the hypothesis that higher hot-water flow rate improves the measured trend (**Figure 3**). The lowest effectiveness value was 0.14 at 1.5 L/min and was treated cautiously as a possible outlier. The low peak effectiveness suggests substantial opportunity for future optimization of heat-transfer area, shell-side flow distribution, purging, and other practical loss mechanisms.

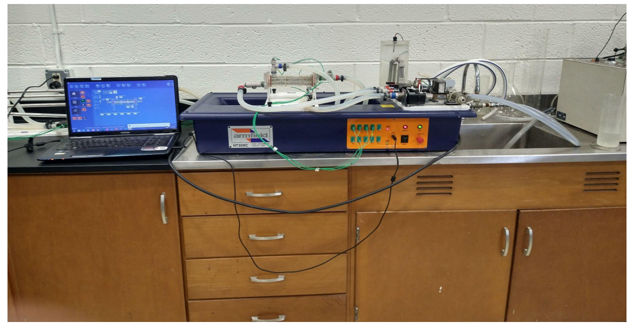

Figure 3. Experimental Setup.

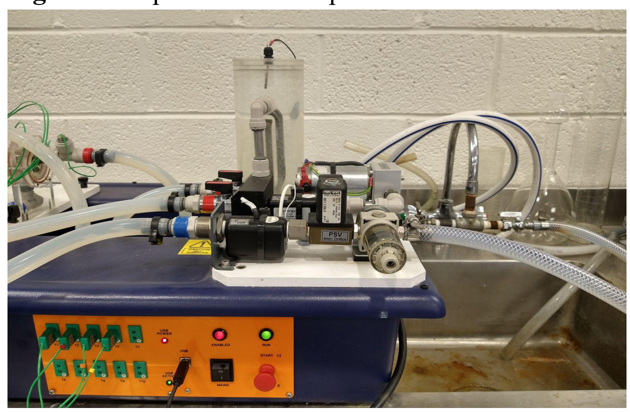

Figure 4. Fluid Circuits and Heater of Heat Exchanger.

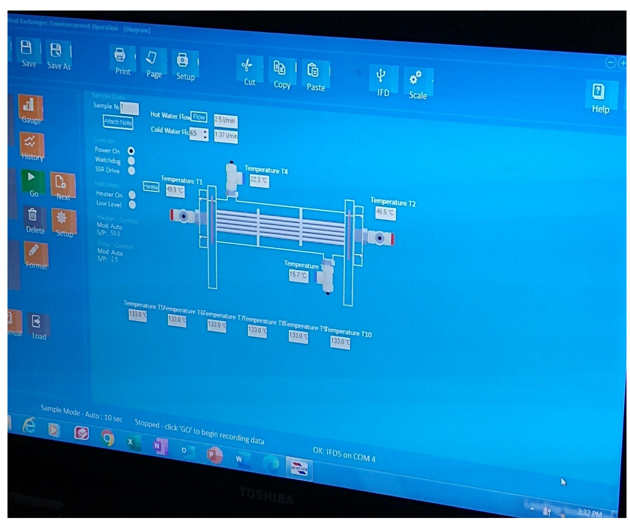

Figure 5. Heat exchanger data collection on HT33 Software.

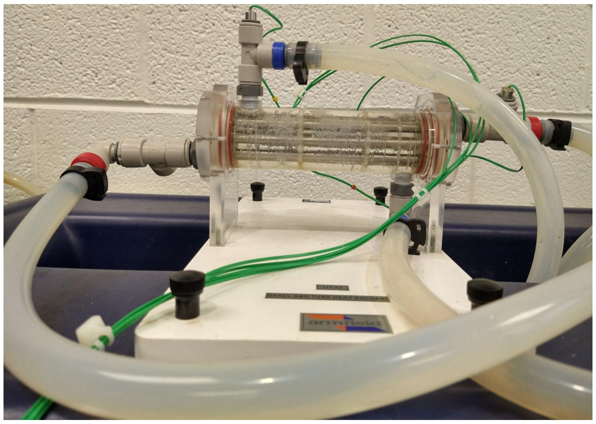

Figure 6. Shell and Tube Countercurrent configuration of HT33X Heat Exchanger.

Table 4. Average Data from Experimentation.

q_h (L/min)	q_c (L/min)	T_1 (°C)	T_2 (°C)	T_3 (°C)	T_4 (°C)
0.5	1.37	50.6	41.1	15.7	19.6
1.0	1.33	50.5	44.6	15.7	20.3
1.5	1.38	51.3	46.6	15.7	21.3
2.0	1.37	50.3	46.4	15.7	21.8
2.5	1.36	50.2	46.4	15.7	22.0
3.0	1.34	50.2	47.2	15.7	22.5
3.5	1.36	49.6	46.9	15.7	23.1
4.0	1.37	49.9	47.5	15.7	23.2
4.5	1.35	49.4	47.2	15.8	23.6
5.0	1.36	49.8	47.9	15.8	23.8

Table 5. Thermal Efficiency (η) and Effectiveness (ε) Calculations

Observation	Fluid Flow rates (q)		Heat Transfer (Q) Calculations				Thermal Efficiency	Heat Capacity (C)			Temperature Gradient (K)		Heat Exchanger Effectiveness
#	hot, q_h (L/min)	cold, q_c (L/min)	$Q_a + Q_r$ (W)	Q_a (W)	Q_r (W)	Q_e (W)	η % = Q_r/Q_e x100%	C_C (W/K)	C_H (W/K)	C_{min} (W/K)	T_{Co}-T_{ci} or, T_{Hi}-T_{Ho} (K)	T_{Hi}-T_{ci} (K)	$\varepsilon = \frac{C_H(T_{Hi}-T_{Ho})}{C_{min}(T_{Hi}-T_{Ci})}$ or $\varepsilon = \frac{C_C(T_{Co}-T_{Ci})}{C_{min}(T_{Hi}-T_{Ci})}$
1	0.5	1.37	369	80.7	288	326	88.6%	95	34	34	2	35	0.15
2	1.0	1.33	426	80.7	346	410	84.2%	93	69	69	4	35	0.16
3	1.5	1.38	531	80.7	450	485	92.8%	96	103	96	5	36	0.14
4	2.0	1.37	582	80.7	502	541	92.7%	95	138	95	4	35	0.16
5	2.5	1.36	594	80.7	513	654	78.5%	95	172	95	4	34	0.20
6	3.0	1.34	630	80.7	550	619	88.7%	94	206	94	3	35	0.19
7	3.5	1.36	699	80.7	619	634	97.6%	95	241	95	3	34	0.20
8	4.0	1.37	710	80.7	629	670	93.9%	95	275	95	2	34	0.21
9	4.5	1.35	729	80.7	648	681	95.2%	94	310	94	2	34	0.22
10	5.0	1.36	756	80.7	675	677	99.9%	95	344	95	2	34	0.22

Q_a : Heat gained by the cold water flowing in the shell from surrounding air

$Q_a + Q_r$: Heat gained by the cold water in the shell from the hot water flowing in the tubes and the heat emitted by the hot water flowing in the tubes

Q_r: Heat gained (received) by the cold water in the shell from the hot water flowing in the tubes minus heat gained from the surrounding air

Q_e : Heat emitted by the hot water flowing in the tubes

Q_m : Maximum possible heat transfer in the heat exchanger calculated from heat capacity

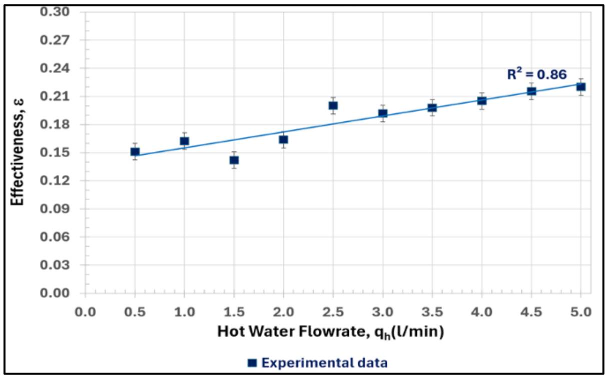

Figure 7. Heat Exchanger Effectiveness vs Hot Water Flow Rate.

Simulation and Experimental Comparison

Simulations were conducted for each experimental flow rate. The simulation and experimental results showed the same increasing trend with hot-water flow rate, but the comparison should be interpreted cautiously because the CFD model was a six-tube simplification of a seven-tube apparatus and used an initial turbulence model that may overpredict mixing in laminar or transitional regions.

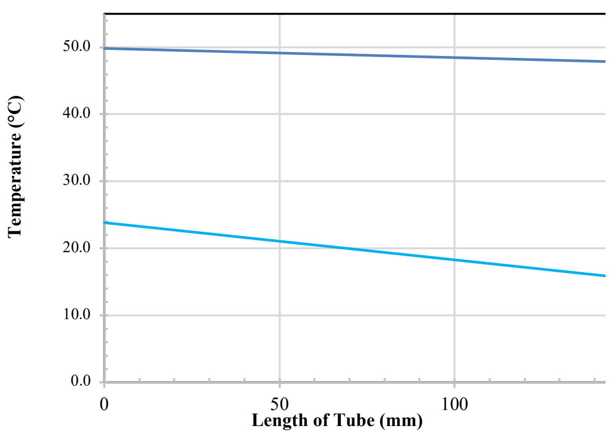

Figure 8. Temperature (°C) vs Length (mm) for Hot and Cold Fluid Flow when q_h = 5.0 L/min.

The trend-line R^2 values describe correlation within each dataset, not exact geometric validation of the CFD model.

The simulation predicted a higher peak effectiveness (approximately 0.28) than the experiment (approximately 0.22) (**Figure 9**). This difference may be associated with the simplified geometry, the absence of experimental air pockets and fouling in the model, and the use of a standard k-epsilon formulation in regions where laminar or transitional behavior may be present.

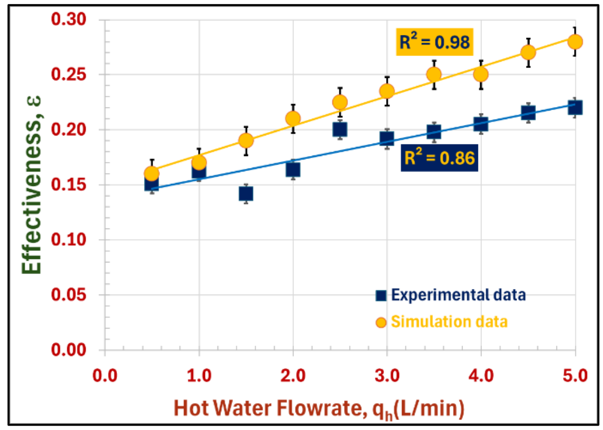

Figure 9. Comparison of Heat Exchanger Effectiveness Between Simulation and Experimentation.

Simulation Contours

Several contours were generated to analyze heat exchanger performance for trials with hot water flow rate set to 5 L/min (highest measured effectiveness).

Figure 12 shows the computed temperature contours in the exchanger. The contours illustrate how heat is transferred from the hot fluid to the tube walls and then to the cold shell-side fluid. Areas with relatively small temperature change or uneven thermal distribution suggest possible limitations in shell-side flow distribution and local heat-transfer area. These contour results are used as qualitative diagnostics for identifying possible redesign opportunities.

Additionally, the hot water remains at a similar temperature between the inlet and outlet ports, deviating in temperature by less than 10 K. Having such minimal heat difference indicates that cold water can uptake more heat than is currently being transferred to it.

Flow mapping of the heat exchanger in **Figure 10** shows the computed flow path through the exchanger, helping visualize recirculation zones and areas of stagnation. The baffles influence the direction and mixing of shell-side flow; better-guided flow may improve local convection by reducing dead zones and increasing contact with the tube surfaces. Velocity vectors inside the tubes also help identify regions where the flow may slow or separate.

Poor flow distribution can lead to uneven heat transfer and fouling in real-world applications, reducing overall thermal efficiency. The contour clearly identifies several areas of concern within this design: there are several areas where flow paths deviate greatly from each other, causing energy losses. Circulation is also especially prominent in the inlet hot water, with the fluid completing several circulations before entering the heat exchange area. Stagnation is also occurring in several areas of the exchanger, creating the need for more turbulent mixing within the heat exchanger.

Pressure contours (**Figure 11**) show that the static pressure at the hot fluid inlet port starts high, with the highest being 30.9 Pa, which gradually decreases within the control volume, reaching down to zero and even as low 10.5 Pa near or at the hot fluid outlet port. In contrast, the cold fluid zone maintains a constant pressure of 0 Pa (with slight variations) throughout its control volume from the cold fluid inlet port, through the control volume, and out the cold fluid outlet port.

The major pressure drop occurs in the hot fluid inlet port, indicating the need for modification to reduce pressure losses.

Additionally, **Figure 13** shows the highest velocity as 0.18 m/s occurring near the outlet port of the hot water, and the lowest velocities are 0.00 m/s, occurring near the walls of the exchanger. Upon inspection, most of the fluid loses a considerable amount of velocity from its entrance into the heat exchanger to its exit. This indicates the need for a redesign to reduce losses in velocity.

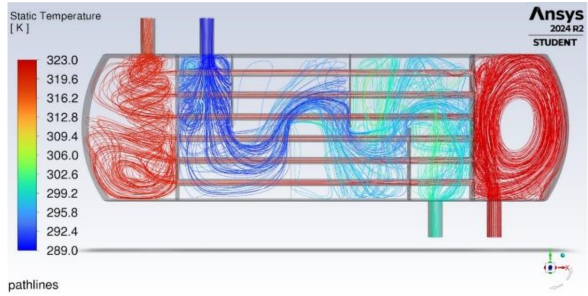

Figure 10. Flow Mapping in the Shell and Tube Heat Exchanger.

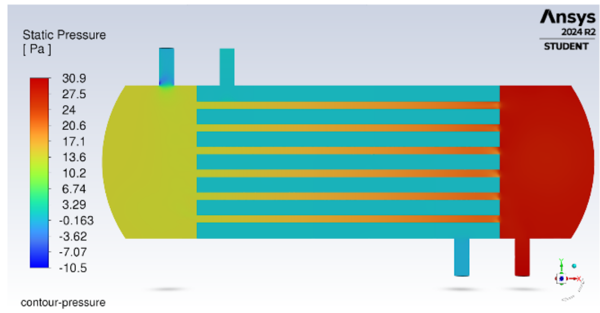

Figure 11. Contours of Pressures in Shell and Tube Heat Exchanger.

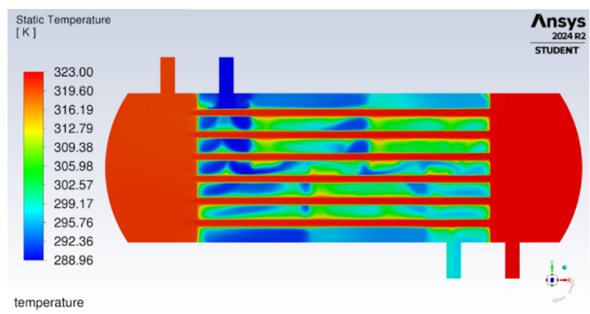

Figure 12. Contours of Temperatures in Shell and Tube Heat Exchanger.

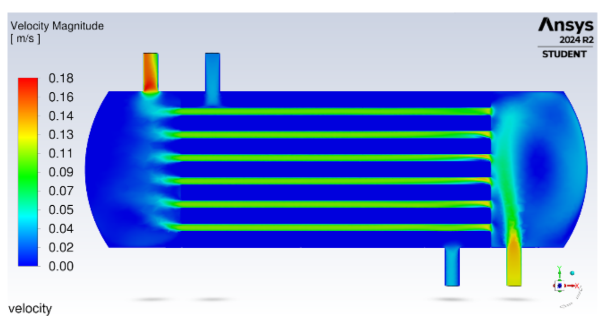

Figure 13. Contours of Velocities in Shell and Tube Heat Exchanger.

Model Comparison and Limitations

The CFD results were compared with experimental results to evaluate whether both approaches showed the same overall trend. Residuals and mass balances were also reviewed as numerical checks. Because the CFD geometry contained six tubes rather than the seven-tube laboratory configuration and because the turbulence model was not reselected based on local Reynolds-number regimes, this comparison is best described as a trend comparison and diagnostic visualization rather than full CFD validation.

Ongoing Future Work

"How can an existing shell and tube heat exchanger be redesigned to create a novel and more thermally effective solution, while maintaining its structural integrity?"

Based on the insights gained from the experiments, simplified CFD contours, and preliminary MATLAB calculations, several future design improvements were identified for further testing. These concepts are proposed as future work and were not fully validated by a new seven-tube conjugate heat-transfer CFD model or by new experiments in this revision:

- Circulation reduction: Strategically placing additional baffles in different orientations may reduce internal circulation and improve heat-transfer performance.
- Increased heat transfer surface area: Expanding the surface area of heat exchange between the two fluids could improve heat-transfer performance.
- Management of recirculation and flow vortices: Placing diagonal, helical, or other flow-tripping baffle geometries at circulation points may help guide shell-side flow and reduce energy losses caused by vortices and dead zones.
- Reduction of stagnation: Extended-surface features and improved baffle arrangements may reduce stagnant zones and promote more uniform heat transfer.
- Structural optimization: Using findings from the experiment and simplified computational visualization, a conceptual redesign was proposed for future validation while maintaining structural feasibility.

Main Aspects of the Novel Heat Exchanger Design

1. U-tube Design:
   - May reduce stagnant regions and allow alternate flow arrangements, depending on manifold and shell-side design.
   - May increase the heat transfer surface area as supported by the heat transfer equation.
   - May enhance overall heat transfer performance while maintaining structural integrity.
2. Diagonal Baffles:
   - Diagonal, transverse, or helical baffle arrangements may improve shell-side flow guidance and increase the outer/shell-side convective heat-transfer coefficient, h_o, thereby improving the overall heat-transfer coefficient, U. Any improvement in the inner tube-side coefficient, h_i, would require separate tube-side flow or geometry modifications.
   - May promote a more uniform heat transfer rate by directing the fluid flow more efficiently.
3. Rounded Entrance/Exit Ports:
   - May reduce frictional losses at the inlet and outlet ports and should be evaluated through future pressure-drop analysis.
   - May reduce pressure drop, allowing higher flow rates without compromising heat transfer efficiency.

The combination of these conceptual design features provides a reasonable future design direction, but it should not be interpreted as a validated final design. A seven-tube conjugate heat-transfer CFD model and follow-up experimental testing are needed to quantify the effect of flow control, increased heat-transfer area, and reduced stagnation without compromising structural integrity.

Strategy/Plan for Improving Heat Exchanger Effectiveness

The primary strategy to enhance the effectiveness of the heat exchanger is to optimize key thermal-fluid variables and minimize energy losses. The following targeted improvements were identified based on experimental observations, computational simulations, and theoretical analysis:

1. Increase Inner Tube Convection Coefficient (h_i):
   - Approach: Increase the hot-water flow rate to increase the Reynolds number and convective mixing within the tubes, which may increase the tube-side convective heat-transfer coefficient, h_i.
   - Impact: Increased Reynolds number and convective mixing may improve heat transfer from the hot fluid to the inner tube walls, thereby improving overall heat-exchanger effectiveness.
2. Increase Outer Tube Convection Coefficient (h_o):
   - Approach: Introduce strategically placed baffles and extended-surface or flow-tripping features within the shell to guide flow, reduce dead zones, and increase contact with the tube surface.
   - Impact: This improves outer tube convection by increasing fluid contact with the tube walls, maximizing heat transfer.
3. Increase Thermal Conductivity of Tube Material:
   - Approach: Select highly conductive tube materials such as copper, aluminum, or other high thermal conductivity alloys.
   - Impact: Higher thermal conductivity reduces thermal resistance, allowing more efficient heat transfer from the hot to the cold fluid.
4. Increase Heat Transfer Surface Area:
   - Approach: Integrate extended-surface features such as integral low-fin tubes, transverse/helical baffles, or other flow-tripping geometries inside the shell-side flow path.
   - Impact: Increased surface area allows for more contact between fluids, improving the heat transfer rate and overall effectiveness.
5. Reduce Fluid Stagnation Zones:
   - Approach: Employ diagonal baffles or fins to reduce stagnation zones within the shell, promoting continuous fluid movement.
   - Impact: Reduced stagnation minimizes heat loss and allows uniform heat distribution across the exchanger surface.
6. Reduce Fouling Effects:
   - Approach: Regularly clean scale deposits or mineral buildup from the inner tube, outer tube, and shell surfaces caused by water impurities.
   - Impact: Reduced fouling ensures unimpeded heat transfer and maintains high effectiveness.
7. Minimize Frictional Head Losses:
   - Approach: Implement rounded and smooth inlet and outlet ports to reduce pressure drop and minimize flow resistance.
   - Impact: Reduced head losses ensure consistent high flow rates without compromising energy efficiency.
8. Reduce Heat Loss to Surroundings:
   - Approach: Select highly insulative shell materials or introduce additional insulation layers to prevent heat loss to the surrounding environment.
   - Impact: Improved insulation enhances the system's overall thermal efficiency.

Theoretical Framework

The combined implementation of these strategies is expected to improve performance by increasing heat-transfer area, improving shell-side flow guidance, and reducing avoidable losses. However, the proposed design should be regarded as a preliminary concept. The fundamental heat-transfer equations and terminology used in this study follow standard heat-transfer and effectiveness-NTU methods (Incropera and DeWitt, 2006; Kakaç and Liu, 2012; Greitzer et al., n.d.). Preliminary Optimization:

Because of the complex interaction among these thermal-fluid variables, MATLAB calculations were used to screen the possible effect of increasing effective heat-transfer area. These calculations were not validated by a new ANSYS Fluent conjugate heat-transfer simulation; therefore, the predicted improvement is reported only as a theoretical estimate requiring future CFD and experimental confirmation.

Modifications for New Design

Following the analysis of the experimental results and simplified CFD contours, a conceptual design (**Figures 14-17**) was formulated to explore possible improvements in overall thermal effectiveness. The concept includes a U-tube-style layout and shell-side flow-guidance features that may increase effective heat-transfer area and reduce stagnant regions. These features are proposed for future design study and should be validated with a seven-tube conjugate heat-transfer CFD model before being treated as a final design.

In this concept, the term "finned baffles" refers to extended-surface or flow-tripping features placed in the shell-side flow path to increase effective heat-transfer area and guide the flow. Future design work should compare this concept with established alternatives such as integral low-fin tubes, transverse baffles, and helical baffles.

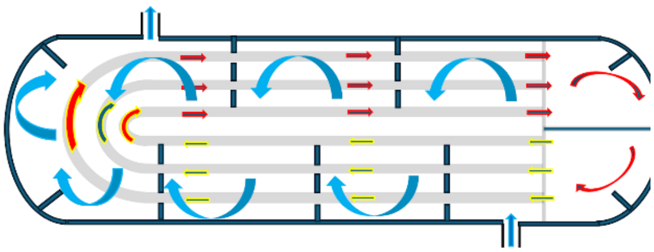

Figure 14. Concept for a New Heat Exchanger Design.

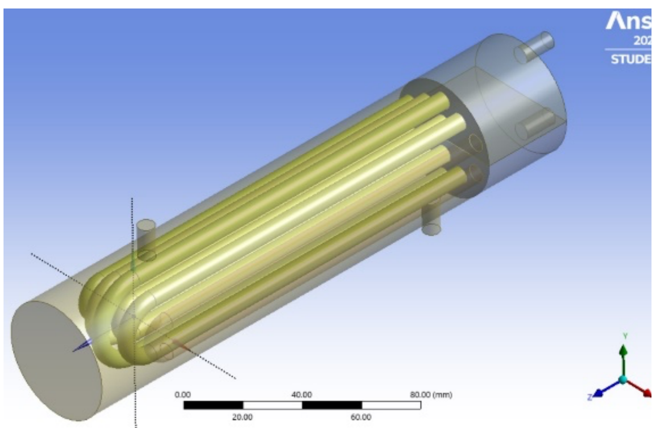

Figure 15. Model 1: 3D Model of U-Tube with Straight and Curved Finned Heat Exchanger

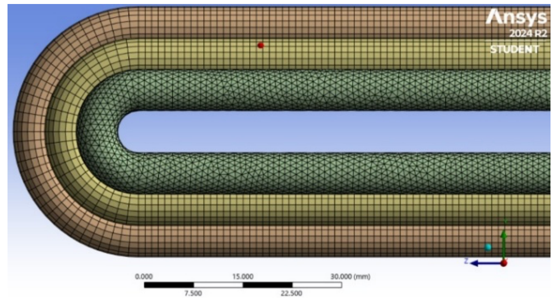

Figure 16. Model 1: 3D Model with meshing of U-Tube with Straight and Curved Finned Heat Exchanger

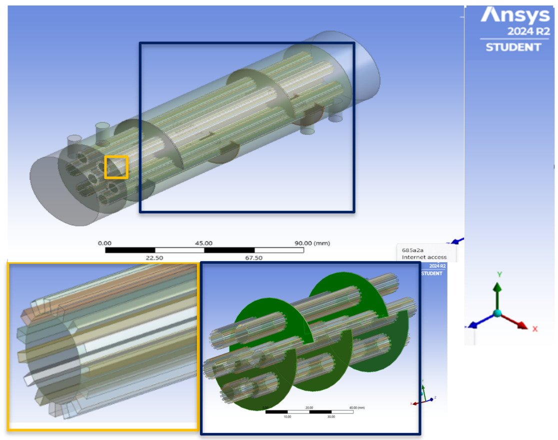

Figure 17. Model 2: Straight Tube Finned Heat Exchanger Model with Zoomed Views of Fins and Baffles

MATLAB Preliminary Screening

The conceptual design was screened using a published MATLAB effectiveness-NTU code (Kokate, 2020) to estimate the potential effect of increasing heat-transfer area.

The MATLAB calculation estimated that increasing effective heat-transfer area to 68,384 mm² could raise effectiveness to approximately 0.56 (**Figure 18**). This value is a theoretical screening result, not an experimentally measured or ANSYS-verified value.

The corresponding estimated inlet and outlet temperature changes for the 68,384 mm² heat-transfer-area case are shown in **Figure 19**.

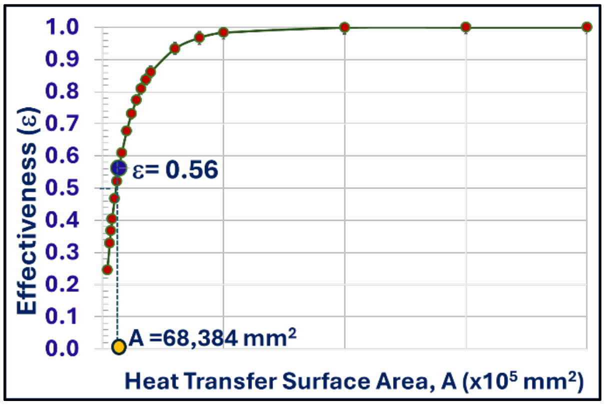

Figure 18. Effectiveness as a Result of Changes in Heat Transfer Area.

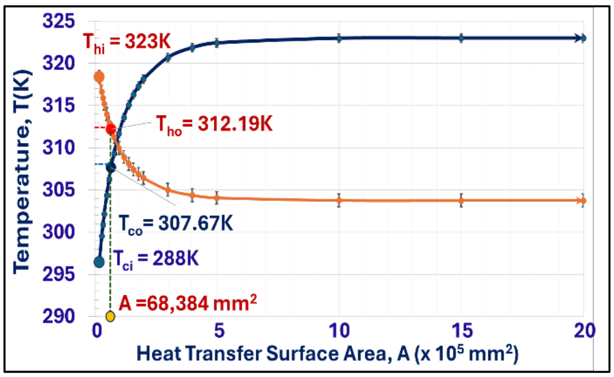

Figure 19. Changes in Temperatures When Heat Transfer Area = 68,384 mm^2.

Discussion

The investigation into the thermal performance of the HT33X shell-and-tube heat exchanger yielded practical insights into the limitations of the current educational apparatus and identified promising pathways for future improvement.

The experimental analysis confirmed that heat transfer occurred from the hotter tube-side fluid to the colder shell-side fluid and that increasing the hot-water flow rate generally increased thermal effectiveness. The peak measured effectiveness was approximately 0.22, which is low for a heat-exchanger system and suggests that heat-transfer area, flow distribution, bypassing, air pockets, fouling, or other practical losses may have limited performance. The relatively high calculated efficiency should therefore be interpreted together with the low effectiveness and the limitations of the apparatus and measurements.

The combined experimental analysis, MATLAB-based screening, and simplified ANSYS Fluent simulations provided a useful framework for diagnosing the existing unit and identifying future design directions. The main performance barriers suggested by the results include limited heat-transfer area, flow stagnation, circulation losses, pressure losses, and possible fouling or air-pocket effects. In response, the proposed design concepts emphasize increased surface area and improved shell-side flow guidance, while recognizing that these concepts require additional verification.

The MATLAB screening calculation suggested that increasing the effective heat-transfer area to 68,384 mm² could theoretically increase effectiveness from approximately 0.22 to approximately 0.56. This estimate highlights the likely importance of heat-transfer area, but it should not be interpreted as a confirmed performance gain because the redesigned geometry was not simulated with a seven-tube conjugate heat-transfer CFD model and was not experimentally tested.

Further flow-control and structural redesign concepts may also be useful. Diagonal, transverse, or helical baffle arrangements could reduce circulation losses and flow vortices, while U-tube or extended-surface configurations may increase thermal interaction area. These proposed changes are best treated as future design hypotheses requiring detailed CFD and experimental verification.

The difference between the experimental peak effectiveness (approximately 0.22) and the simplified CFD peak effectiveness (approximately 0.28) underscores the importance of practical losses and modeling assumptions. Possible contributors include air pockets, fouling, pressure instabilities, heat exchange with the surroundings, the six-tube computational simplification, and the use of standard k-epsilon modeling in potentially laminar or transitional regions. Future simulations should use the measured seven-tube geometry, appropriate flow-regime-specific models, and conjugate heat-transfer treatment.

Future work should refine the conceptual U-tube or extended-surface design, conduct a geometrically matched seven-tube conjugate heat-transfer CFD simulation, and validate the redesigned unit experimentally after careful purging and priming of the apparatus. Future studies should also evaluate pressure drop, manufacturability, material selection, insulation, and fouling control rather than optimizing effectiveness alone.

In conclusion, increasing the hot-water flow rate generally improved the measured effectiveness of the HT33X shell-and-tube heat exchanger, but the maximum experimental effectiveness remained low at approximately 0.22. The simplified CFD model provided useful qualitative insight into possible stagnation, pressure-loss, and flow-distribution issues, while MATLAB screening suggested that increasing effective heat-transfer area could substantially improve theoretical effectiveness. These findings support surface-area enhancement and improved shell-side flow guidance as promising directions, but the proposed redesign requires future seven-tube conjugate heat-transfer CFD and experimental validation before quantitative performance claims can be made.
Overall, this work provides a preliminary, educationally appropriate framework for combining experiments, CFD visualization, and MATLAB screening to study heat-exchanger performance and identify defensible next-step design improvements.

Acknowledgements

The authors would like to thank James Hoffman, Lab Manager at the WVU Tech Engineering Lab, for his valuable assistance with data collection.

Literature Cited

ANSYS FLUENT 12.0 Theory Guide. (n.d.). *Retrieved October 17, 2024, from* https://www.afs.enea.it/project/neptunius/docs/fluent/html/th/main_pre.htm

Bell, K. J. (January 26, 2005). "Heat Exchanger Design for the Process Industries ." ASME. *J. Heat Transfer*. December 2004; 126(6): 877–885. https://doi.org/10.1115/1.1833366

Greitzer, E. M., Spakovszky, Z. S., & Waitz, I. A. (n.d.). 18.5 Heat Exchangers. *Retrieved August 15, 2024, from* https://web.mit.edu/16.unified/www/FALL/thermodynamics/notes/node131.html#eq10:HeatExchTemperatureRatioExp

Incropera, F. P., & DeWitt, D. P. (2006). *Fundamentals of Heat and Mass Transfer* (6th ed.). John Wiley & Sons.

Kakac, S., & Liu, H. (2012). *Heat exchangers: Selection, rating, and thermal design* (2nd ed.). CRC Press.

Kern, D. Q., 1950, Process Heat Transfer, McGraw-Hill Book Company, New York.

Kline, S. J., & McClintock, F. A. (1953). Describing uncertainties in single-sample experiments. Mechanical Engineering, **75**(1), 3-8.

Kokate, R. (2020). *Heat Exchanger using E-NTU method*. MATLAB Central File Exchange. *Retrieved February 25, 2025, from* https://www.mathworks.com/matlabcentral/fileexchange/83863-heat-exchanger-using-e-ntu-method

Menter, F. R. (1994). Two-equation eddy-viscosity turbulence models for engineering applications. AIAA Journal, **32**(8), 1598-1605.

Mohammadzadeh, A.M., Jafari, B., Hosseinzadeh, K. *et al.* Numerical investigation of segmental baffle design in shell and tube heat exchangers with varying inclination angles and spacing. *Sci Rep* **15**, 4683 (2025). https://doi.org/10.1038/s41598-025-87652-x

Prithiviraj, M., & Andrews, M. J. (1998). Three Dimensional Numerical Simulation of Shell-and-Tube Heat Exchangers. Part I: Foundation and Fluid. *Numerical Heat Transfer, Part A:*

Applications, ***33***(8), 799–816. https://doi.org/10.1080/10407789808913967

Rodrigues, G., & Srivastava, N. (2024). Comparative study between Finite Volume Method and Analytical Method to Analyse Thermal Efficiency of Double-Pipe Heat Exchanger. *Case Studies in Thermal Engineering*, 105713.

https://doi.org/10.1016/j.csite.2024.105713

Tayyab, M., Awan, D. A., and Shah, A. (December 9, 2024). "Design Optimization of a Shell-and-Tube Heat Exchanger Based on Variable Baffle Cuts and Sizing." ASME. *J. Thermal Sci. Eng. Appl*. February 2025; **17**(2): 021008. https://doi.org/10.1115/1.4067235